Effect of Time Delays and Sampling in Force Actuated Real-Time Hybrid Testing; A Case Study

Einar S. Ueland
Centre for Autonomous Marine Operations and Systems (NTNU AMOS)
Department of Marine Technology
Norwegian University of Science and Technology (NTNU)
NO-7491 Trondheim, Norway
Email: einar.s.ueland@ntnu.no

Roger Skjetne
Centre for Autonomous Marine Operations and Systems (NTNU AMOS)
Department of Marine Technology
Norwegian University of Science and Technology (NTNU)
NO-7491 Trondheim, Norway

***Abstract*—This paper presents a study where real-time hybrid testing is applied on a double mass-damper-spring system. Simulations show how delays and sampling terms affect the system both when it is subjected to excitations forces and in free decay. In particular, it is shown how the stiffness of the actuator combined with time delays can have a profound effect on the real-time hybrid test case. Further, using the test case, first order Taylor expansions are used to show how linear stiffnesses combined with delays can be approximated as linear damping terms, while linear damping terms can be approximated as added mass terms. These approximations are useful in providing intuitive insight into how delays will affect the real-time hybrid test system.**

I. Introduction

Hybrid testing is a method where experimental testing of a physical substructure is combined with numerical substructures that emulate the parts of the structure that are not modeled physically. Typical for hybrid testing is that components that are complex or highly nonlinear are tested physically, while components that are well understood are emulated numerically. The numerical and physical substructures are coupled, through a measurement interface and an effort interface that applies the corresponding effort (e.g. forces, displacements, etc.) onto the physical substructure.

This paper is part of a larger research campaign, where real-time hybrid testing is being developed for use in hydrodynamic model testing. Within this field, to emphasize that hybrid tests are performed at model scale, and in real-time, the denomination *Real-Time Hybrid Model testing* or *ReaTHM® testing*[1] is used. In this context "real-time" refers to the real-time constraints that are needed in connecting the numerical and physical substructures, to ensure an accurate behavior of rate dependent factors. This paper we will generally refer to this as hybrid testing.

Hybrid testing for marine phenomena often involve tests where the environmental loads result in relatively large motions of the structure; see for example [1]. For this reason, the actuators must be able to handle relatively large motions of their end effectors relative to their fixed suspension points. Also, due to the dynamics of the marine structures, it is often necessary to actuate the effort calculated by the numerical model as forces and moments on the physical system. This implies that methods for force actuation in the hybrid test-loop are needed. The paper will use a simple test case of a double mass-damper-spring system to investigate how time delays and sampling affects the force actuation of the system, with the goal of improved understanding of how these factors affect the test performance. The overall goal is to obtain a fundamental understanding of limitations in the real-time hybrid test loop, that hopefully also can be applied to more complex hybrid test cases.

The paper is motivated by challenges related to force actuation and time delays experienced in previous applications of hybrid testing for marine applications. Although the test case investigated is simpler, and not marine specific, the general structure of the hybrid test-loop and the actuator in use is similar to those used in previous applications, see for example [2]. Since the objective of the research performed in the paper is to further the development of hybrid testing for marine environments, the paper will repeatedly refer to and relate results to marine applications, even though the test case itself, strictly speaking, is not marine.

II. The Hybrid Test Loop

The hybrid test loop, which for this paper is structured as illustrated in Figure 1 is a closed-loop system, where the physical and numerical substructures are excited by each other. Typically, the effect that the physical system has on the numerical system is estimated based on sensor measurements, while the effect that the numerical system has on the physical is actuated through an actuation interface. In the hybrid test loop of Figure 1, the states of the physical system are denoted

[1] *ReaTHM® testing* is a registered trademark of SINTEF Ocean.

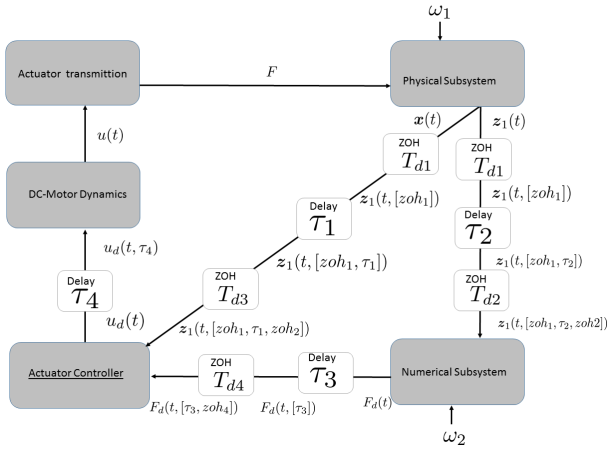

Figure 1: Hybrid Test Loop, with delays and zero-order-hold elements indicated

z_1, and (although not present in the figure) the states of the numerical substructure will be denoted z_2. Note that this paper does not investigate the effect of measurement and observation errors, which, therefore, are not included in the Figure. In the following sections, each of the components of Figure 1 will be elaborated.

A. Substructures

1) Physical substructure: Typical for real-time hybrid testing is that effects and structures which are complex or highly nonlinear need to be tested physically. Within marine applications, a typical example is the effects of hydrodynamical phenomena that occur near the free surface of the water.

2) Numerical substructure: Due to the complexity of structures, limitations of facilities, or conflicting scaling laws, it is not always practical to perform tests of the whole structure; see for example [3]. Components that one can model numerically with a sufficient accuracy, and which are difficult to include in the physical tests are emulated numerically. In more complex systems, the numerical substructure, may, for example, be nonlinear finite element program, that runs on a separate, dedicated computer.

B. External Loads

In general, external loads may act on both the numerical and the physical substructure. The hybrid test loop of Figure 1 separates between a load vector ω_1 which acts on the physical substructure and load vector ω_2 which acts on the numerical substructure. In marine applications, hydrodynamical loads, are typically important components of ω_1 (while the ω_2, for instance, may be loads acting on numerically simulated mooring lines).

C. Time Delays

In general, due to sampling, processing, synchronization, and communication times, time delays are present in the hybrid test loop. Figure 1 separates between four delays; τ_1 and τ_2 which is the delay of the physical states, when used by the actuator controller and numerical substructure respectively, τ_3, which is the delay from the numerical substructure to the physical substructure, which for more complex models, typically is dominated by the processing time, and τ_4, which relates to the delay between calculated desired motor input and the response of the motor. In hybrid testing applications, the time delays should be kept to a minimum, yet as will be shown, even small time delays may have a considerable effect on the closed-loop hybrid system. See [4] for an example where time delays are discussed in the context of real-time hybrid model testing on offshore systems in deep water.

D. Zero-order-holds

Figure 1 further indicates four zero-order-hold (ZOH) blocks, which are the sample and hold elements induced by information being sampled at a constant frequency. It is separated between four different ZOH elements; T_{d1}, which corresponds to the digitalization of measurements performed through a data acquisition system, T_{d2}, which is the sampling period for which the numerical substructure sample new data, then T_{d3} and T_{d4}, which is the sampling period for which the physical states and force reference feedforward term, z_1 and F_d respectively, are sampled by the actuator controller.

It will be assumed that the internal numerical model is solved continuously during a time-step, meaning that there is no ZOH discretization of the states in the numerical substructure. The outputs of the numerical substructure are however still processed by the corresponding ZOH element T_{d2}, as it is outputting data at the same frequency as the block inputs data.

In this paper, a function $f(t)$ affected by a ZOH element T_{d1} is denoted $f(t, zoh_1)$, while a signal delayed by τ is denoted $f(t,\tau)$. With a slight abuse of notation, for the sake of compactness, a signal affected by a combination of several ZOH-elements and delays it is denoted $f\left(t,\left[T\right]\right)$, where T is a sequence of ZOH and delays. An example of this denotation, and how these elements affect a signal $f(t)$ can be seen in Figure 2. In this example, the trajectory of $f(t)$ is processed by two ZOH elements and one time delay. Note that, for the sake of compression, the paper will repeatedly skip the dependency of t for functions that are not delayed. (ie. $f(t) = f$)

All time delays and ZOH elements are in this paper estimated as constant, and there is no freeze error occurring w.r.t. signal transfer. The effect of a ZOH element affecting an already discretized signal is that we get a varying hold element. In Figure 2 this effect is illustrated by T'_{d3}, which is the hold time that affects the discretized sample. Typically, in real-time applications, the sampling rates are synchronized and sequenced, such that the effect of the second ZOH element is limited.

E. Actuation System

The actuator is responsible for applying the desired force to the physical substructure. The actuators should both reject disturbances (force actuation should not be dependent on the movement of the end effectors), and be able to apply the

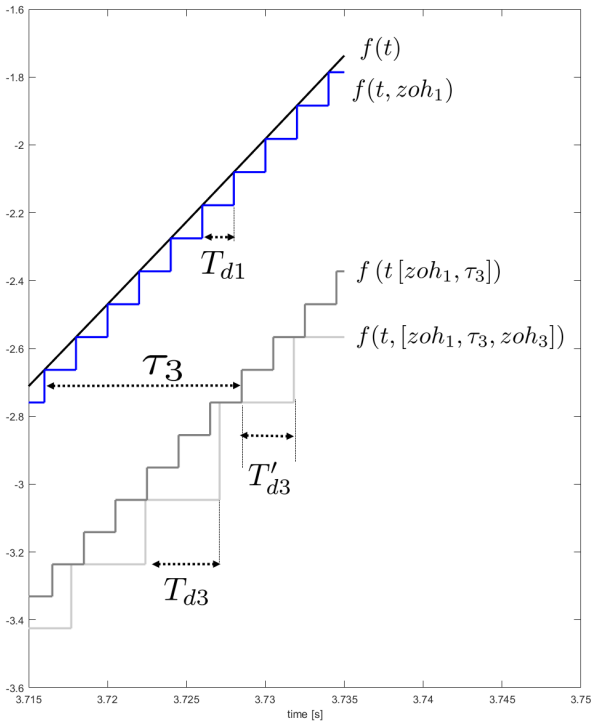

Figure 2: Sampling and delay effect illustrated for a sample signal $f(t)$

desired forces on the structure. The actuator consists of a DC-motor, connected via a compliant transmission system to the physical substructure where force is applied. In this project, the force actuation system is modeled based on a similar actuator to the one used in [5].

1) DC motor dynamics: The DC motor illustrated in Figure 3 is assumed to have an internal servo-controller, where only basic parameters can be tuned. Due to the internal dynamics of the motor, which is driven in position mode, there will be a transient phase between the desired input u_d and the output u, which in the Laplace-plane is modeled as the transfer function $H(s)$. In this paper the transfer function of the DC-motor will be modeled as in [6, Section 3.5], which models the open loop control of a DC motor as a first order process, while the closed-loop position control is modeled as a second order process combined with a time delay:

$$H(s) = e^{-\tau_4 s} h(s) \tag{1}$$

where,

$$h(s) = \frac{1}{(1 + \frac{s}{k_v})(1 + \frac{s}{k_a})} \tag{2}$$

where it is assumed that $k_a >> k_v$.

Note that many DC-motors, in reality, have a somewhat more complex model, where typically also the load factor is an important parameter affecting the motor performance. However, the simpler model offers the advantage of being simpler to fit, as it has only two parameters.

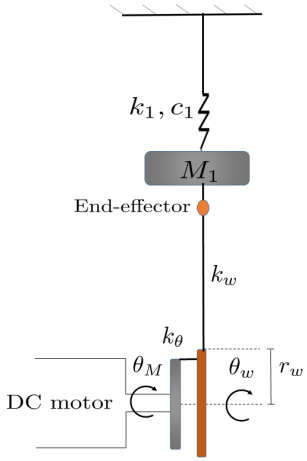

Figure 3: The actuator connected to the physical substructure, which in this case consists of a mass M_1 connected via a spring K_1 to the rigid roof.

2) Actuator Transmission System: The DC-motor shaft is connected to a wheel pulley via a clock spring, as illustrated in Figure 3. As the clock spring is deflected, a torque will be generated and transformed to a linear force in a wire connected to the wheel pulley. This wire is again connected to the physical system via a strain-gauge. The wheel pulley allows for wire to be pulled in and out, facilitating for force control, even with large movements of the end-effector

The clock spring element is approximated as a linear torsion spring, with a stiffness k_θ, which is assumed to be accurate as long as there is no contact between the coils of the spring. The wire connecting the wheel pulley to the physical system is pre-tensioned and is modeled as a linear spring with stiffness k_w. The inertia of the system with respect to the angular rotation of the wheel and is estimated as I. Further, a linear damping coefficient c_θ on the rotation is modeled.

The equation of motion for angular rotation of the wheel pulley becomes;

$$\ddot{\theta}_w I + c_\theta \dot{\theta}_w + r_w k_w (\theta_w r_w - x_1) = k_\theta (\theta_m - \theta_w) \tag{3a}$$

$$F = (\theta_w r_w - x_1) k_w, \tag{3b}$$

where θ_w and θ_m are the angular position of the wheel pulley and motor shaft respectively, x_1 and F are the position and force of the end-effector which is connected to the physical mass, and r is the radius of wheel pulley.

Note that the end effector cannot actuate negative forces, as the wire would go slack. However, the wire typically has tension in equilibrium, from which both positive and negative forces can be applied.

3) Force control: In this paper, we will investigate the case where the inertia and damping of (3) can be neglected. If the inertia and damping levels are low, this may be a good approximation for low frequencies outside the natural modes of the transmission system.

With this assumption, (3) reduces to a static model where the generated force is proportional to the stiffness of the system, multiplied with the deflection:

$$F = (u - x_1)k_{tot} + \epsilon \tag{4}$$

where

$$k_{tot} = \left(\frac{1}{k_w} + \frac{1}{k_\theta r_w}\right)^{-1} \tag{5}$$

and where we, for convenience, introduced $u = \theta_m r$ as the control variable of the DC-motor, which is driven in position mode. Further, all errors, including mechanical vibrations and modeling inaccuracies are lumped into the error term ϵ.

For the further analysis, we make the assumption that the desired control input is the one that would yield correct force given instantaneous and error-free actuation. The controller is separated into three terms; a position cancellation term $u_{d,fx}$, a reference feedforward term $u_{d,ff}$, and a constant deflection term u_0 corresponding to a pre-tensioned equilibrium. This gives:

$$u_d = u_{d,ff} + u_{d,fx} + u_0 \tag{6a}$$
$$u_{d,fx} = x_1 \tag{6b}$$
$$u_{d,ff} = \frac{F_d}{k_{tot}}, \tag{6c}$$

where F_d is the desired force that we wish to track.

The resulting actuator force is similarly separated into a position cancellation term F_{fx}, a force-tracking term: F_{ff}, and a constant pretension term F_0 . That is :

$$F = F_{fx} + F_{ff} + F_0 + \epsilon \tag{7a}$$
$$F_{fx} = \big(u_{d,fx}H(s) - x_1\big)k_{tot} \tag{7b}$$
$$F_{ff} = H(s)u_{d,ff}k_{tot} \tag{7c}$$
$$F_0 = u_0 k_{tot}, \tag{7d}$$

where ϵ is the error term introduced in (4)

III. Real-Time Hybrid test-case: Lumped mass-damper-spring system

The aim of this study is to improve understanding of the hybrid test loop through investigation of a well-understood system. The system of Figure 4, which is a lumped double mass-damper-spring system, can be tested through hybrid testing, using the experimental setup of Figure 3. The system is modeled as a linear system, assuming that no out-of-plane oscillations affect the system. The position of the two masses are denoted x_1 and x_2 for mass M_1 and mass M_2 respectively, while the difference $(x_1 - x_2)$ is denoted $\tilde{x}$. The system equations are:

$$M_1\ddot{x}_1 + c_1\dot{x}_1 + c_2\dot{\tilde{x}} + k_1x_1 + k_2\tilde{x} = \omega_1 + M_1 g \tag{8a}$$
$$M_2\ddot{x}_2 + c_3\dot{x}_2 - c_2\dot{\tilde{x}} + k_3x_2 - k_2\tilde{x} = \omega_2 + M_2 g \tag{8b}$$

The forces acting on each mass is now split into two parts. F_c is the part of the force acting in the interface between the two masses, while ΣF_1 and ΣF_2 , are the sum of forces excluding F_c, acting on the M_1 and M_2 respectively. Further, x_1 and x_2 are defined such that they are zero at equilibrium in steady state, thus eliminating gravity forces from the equations. This yields:

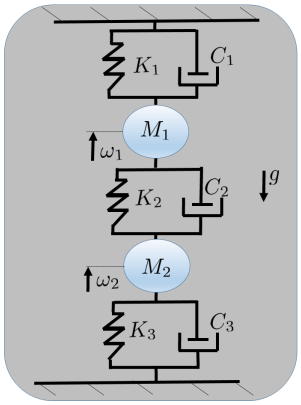

Figure 4: Lumped double mass-damper-spring system

$$M_1\ddot{x}_1 = \Sigma F_1 + F_c \tag{9a}$$
$$M_2\ddot{x}_2 = \Sigma F_2 - F_c \tag{9b}$$

where

$$\Sigma F_1 = -c_1\dot{x}_1 - k_1x_1 + \omega_1 \tag{10a}$$
$$\Sigma F_2 = -c_3\dot{x}_1 - k_3x_1 + \omega_2 \tag{10b}$$
$$F_c = -c_2\dot{\tilde{x}} - k_2\tilde{x} \tag{10c}$$

Note that due to the redefinition of x_1 and x_2, we have also redefined the control input u about the equilibrium u_0.

For further analysis, to separate it from its hybrid counterpart, the system as described in (9) will be referred to as the ideal system.

A notable study performed on mass-damper-spring systems within real-time hybrid testing is [7]. In this study, however, the system substructuring included the interconnection as part of the physical substructure (corresponding to keeping C_2 and k_2 as part of the physical substructure), allowing for position tracking of the numerical mass, rather than force tracking.

A. Substructuring; Numerical and physical substructures

The double mass-damper-spring system is now split into a numerical and physical substructure, as illustrated in Figure 5a. In real-time hybrid testing, the numerical substructure is further replaced with an actuator connected to a computer as seen in Figure 5b. The hybrid test loop for this case is illustrated in Figure 6.

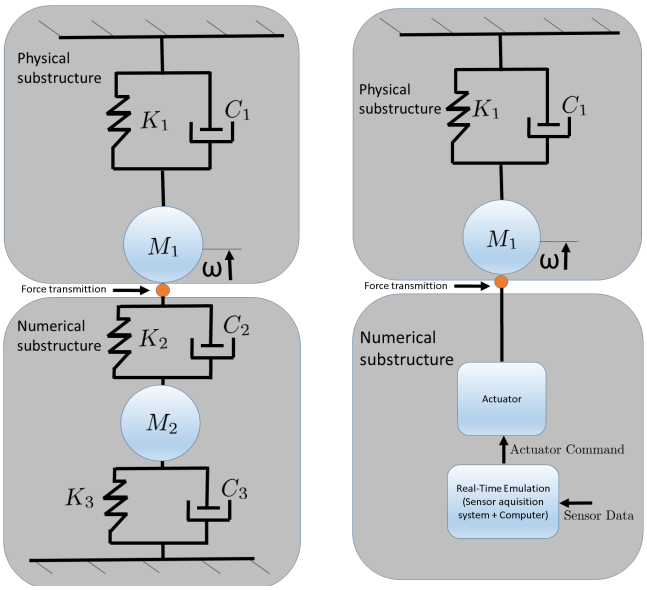

(a) Substructuring (b) Hybrid system

Figure 5: Substructuring with force actuator interface.

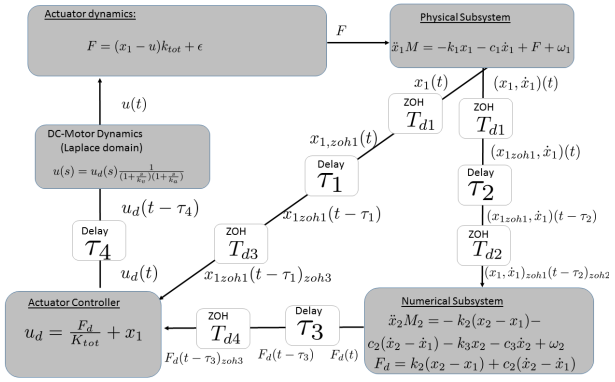

Figure 6: Hybrid test loop for mass-damper-spring system

We now get the following relationships between delayed signals in our hybrid loop:

$$u = u_d(t, \tau_4)h(s) \tag{11a}$$
$$u_{d,x} = x_1(t, [zoh_1, \tau_1, zoh_3]) \tag{11b}$$
$$u_{d,f} = \frac{F_d(t, [\tau_3, zoh_4])}{k_{tot}} \tag{11c}$$
$$F_d(t) = F_c(\boldsymbol{z}_1(t, [zoh_1, \tau_2, zoh_2]), \boldsymbol{z}_2(t, zoh_2)) \tag{11d}$$

Where we used:

$$\boldsymbol{z}_1 = \begin{bmatrix} x_1 \\ \dot{x}_1 \end{bmatrix}, \boldsymbol{z}_2 = \begin{bmatrix} x_2 \\ \dot{x}_2 \end{bmatrix} \tag{12}$$

Also, for the function F_c, then $F_c\Big(z_1(t, T_1), z_2(t, T_2)\Big)$ implies that the trajectories z_1 and z_2 , that are parameters of F_c are affected by T_1 and T_2, respectively.

B. Forces induced from the hybrid system

When comparing the hybrid test system with the ideal system that we want to replicate, noise, time delays, actuator dynamics, etc., inevitably introduce errors in the interaction between the two masses. These errors are denoted ΔF_{num} and ΔF_{ph} for the error on the applied force on the numerical and physical parts respectively. The equation of (9) is then reformulated to account for the errors:

$$M_1\ddot{x}_1 = \Sigma F_1 + F_c + \Delta F_{\text{ph}} \tag{13a}$$
$$M_2\ddot{x}_2 = \Sigma F_2 - F_c + \Delta F_{\text{num}}, \tag{13b}$$

with $F_c, \Sigma F_1,$ and ΣF_2 as defined in (10).

The introduced errors can be expressed as:

$$\Delta F_{\text{num}} = F_c(z_1(t, [zoh_1, \tau_2, zoh_2]), z_2(t))) - F_c \tag{14a}$$
$$\Delta F_{\text{ph}} = F_{fx} + F_c - F_{ff} + \epsilon \tag{14b}$$
$$F_{fx} = (u_{d,x}(t, \tau_4)h(s) - x_1)k_{tot}$$
$$= (x_1(t, [zoh_1, \tau_1, zoh_3, \tau_4])h(s) - x_1)k_{tot} \tag{14c}$$
$$F_{ff} = k_{tot}u_{d,ff}(t, \tau_4)h(s)$$
$$= F_c\Big((z_1(t, [zoh_1, \tau_2, zoh_2]), z_2(t, zoh_2)), [\tau_3, zoh_4, \tau_4]\Big)h(s) \tag{14d}$$

IV. Time delays and sampling approximated through first order Taylor expansion

In order to gain insight into how time delays and ZOH elements affect the system, this section will approximate the hybrid system as linear through the help of first order Taylor expansions.

A. First order Taylor expansion of time delays

Delayed functions can, under certain circumstances be approximated through a Taylor series expansion of the delayed term τ about zero [8], by:

$$f(t - \tau) = \sum_{n=0}^{N} \frac{f^{(n)}(t)}{n!}(-\tau)^n + R(t, \tau, N) \tag{15a}$$

Where the remainder is:

$$R(t, \tau, N) = (-1)^{N+1}\frac{1}{(N+1)!}\tau^{N+1}f^{N+1}(t - \theta\tau) \tag{16}$$

with $\theta \in [0, 1]$, and with the superscript $^{(n)}$ being the n'th derivative of f.

By setting $N = 1$, and by neglecting the term $R(t, \tau, N)$ one arrive at a first order approximation:

$$f(t - \tau) \approx f(t) - \tau\dot{f}(t) \tag{17}$$

1) Zero Order Hold Approximation: A ZOH element with sample size of T_d, can be expressed as a time-varying delay $\tau_{td}(t)$, that on the sampling interval is increasing linearly with time from zero to T_d, before it reaches a new sample time and the time delay is reset to zero.

When the ZOH element occurs on a smooth signal, it can thus be approximated through the first order Taylor expansion on the sampling interval $t \in [t_0 - T_d, t_0]$ as follow:

$$f(t, zoh) \approx f(t) - \tau_{td}(t)\dot{f}(t) \tag{18}$$

Since $\tau_{td}(t)$ is increasing linearly on the sampling interval, we see that that $\tau_{td}(t)\dot{f}(t_0)$ integrated over the sampling interval can be expressed as follows:

$$\int_{t_0-T_d}^{t_0} \tau_{td}(t)\dot{f}(t_0) = \int_{t_0-T_d}^{t_0} \frac{T_d}{2}\dot{f}(t_0) \tag{19}$$

For our purposes, $\left(\dot{f}(t_0)\frac{T_d}{2}\right)$ typically represents a force, and if we assume that the velocity is constant on the interval, the induced energy will be the same in both cases of (19). With this reasoning, the ZOH element of the small hold time T_d on a smooth signal, is approximated as a time delay of $\frac{T_d}{2}$

For the case where the delays or ZOH occur on a nonsmooth signal, already digitalized by another ZOH element, the above arguments will in general not hold.

2) Combining time delays and ZOH elements: Now looking at the ZOH elements, we have T_{d1} which is acting on smooth signals, thus being approximated as $\frac{T_{d1}}{2}$. We will also approximate T_{d2} and T_{d3} as $\frac{T_{d2}}{2}$ and $\frac{T_{d3}}{2}$ respectively, even though ZOH T_{d1} has made the signal non-smooth. The reasoning is that the sampling rate T_{d1} is expected to be much faster than that of T_{d3} and T_{d2}.

We further assume that the numerical substructure is synchronized with the actuator controller, such that the actuator controller is updating each time it receives new data from the numerical substructure. Thus T_{d4} is set to zero. The delays are now lumped together with the ZOHs as follows:

$$T_{d4} = 0 \tag{20a}$$
$$\tau_1' = \tau_1 + \frac{T_{d1}}{2} + \frac{T_{d3}}{2} \tag{20b}$$
$$\tau_2' = \tau_2 + \frac{T_{d1}}{2} + \frac{T_{d2}}{2} \tag{20c}$$
$$\tau_3' = \tau_3 + \frac{T_{d2}}{2} \tag{20d}$$
$$\tag{20e}$$

3) Approximated system: The errors that the substructuring introduces to our system, can be estimated using the first order Taylor approximations;

$$\begin{aligned}\Delta F_{num}(t) &\approx \big(F_c\big(z_1(t,\tau_2'),z_2(t)\big) - F_c \approx -\tau_2'\left(\frac{\partial}{\partial \boldsymbol{z}_1}(F_c)\dot{\boldsymbol{z}}_1^T\right)\\ &= -\tau_2'\big(k_2\dot{x}_1 + c_2\ddot{x}_1\big)\end{aligned} \tag{21a}$$

$$\Delta F_{ph} = F_{fx} + F_c - F_{ff} + \epsilon \tag{22a}$$

where

$$\begin{aligned}F_{fx}(t) &\approx \big(x_1\big(t-\tau_1'-\tau_4\big)h(s) - x_1\big)k_{tot}\\ &\approx -k_{tot}\left(\big((\tau_1'+\tau_4)\frac{\partial}{\partial \boldsymbol{z}_1}(F_{fX})\dot{\boldsymbol{z}}_1\big)h(s)\right) + \big(h(s)-1\big)x_1\\ &\approx -k_{tot}(\tau_1'+\tau_4)\dot{x}_1 h(s) + \big(h(s)-1\big)x_1\end{aligned}$$

and

$$\begin{aligned}F_{ff} &\approx F_c\Big(z_1(t-\tau_2'-\tau_3-\tau_4), z_2(t-\tau_3'-\tau_4)\Big)h(s)\\ &\approx Fc - \left((\tau_2'+\tau_3+\tau_4)\frac{\partial}{\partial \boldsymbol{z}_1}(F_{ff})\dot{\boldsymbol{z}}_1 + (\tau_3'+\tau_4)\frac{\partial}{\partial \boldsymbol{z}_2}(F_{ff})\boldsymbol{z}_2\right)h(s)\\ &\approx F_c + \Big((\tau_3'+\tau_4)\big(c_2\dot{x}_2 + k_2x_2\big) - (\tau_2'+\tau_3+\tau_4)\big(k_2x_1 + c_2\dot{x}_1\big)\Big)h(s)\end{aligned} \tag{24a}$$

In order to do a separate investigation on the effect of time delays and sampling, we will now assume that there are no motor dynamics, meaning that $h(s)$=1. The linear Taylor approximations now yield the following system:

$$\boldsymbol{M}\ddot{\boldsymbol{x}} + \boldsymbol{C}\dot{\boldsymbol{x}} + \boldsymbol{K}\boldsymbol{x} = \boldsymbol{F} + \boldsymbol{\epsilon} \tag{25}$$

where,

$$\boldsymbol{M} = \begin{bmatrix} M_1 - c_2(\tau_2'+\tau_3+\tau_4) & +c_2(\tau_3'+\tau_4) \\ +c_2\tau_2' & M_2 \end{bmatrix} \tag{26a}$$

$$\boldsymbol{C} = \begin{bmatrix} c_1 + c_2 - k_2(\tau_2'+\tau_3+\tau_4) + k_{tot}(\tau_1'+\tau_4) & -c_2 + k_2(\tau_3'+\tau_4) \\ -c_2 + k_2(\tau_2') & c_2 + c_3 \end{bmatrix} \tag{26b}$$

$$\boldsymbol{K} = \begin{bmatrix} k_1+k_2 & -k_2 \\ -k_2 & k_2+k_3 \end{bmatrix} \tag{26c}$$

$$\boldsymbol{F} = \begin{bmatrix} \omega_1 & \omega_2 \end{bmatrix}^T \tag{26d}$$

$$\boldsymbol{x} = \begin{bmatrix} x_1 & x_2 \end{bmatrix}^T \tag{26e}$$

$$\boldsymbol{\epsilon} = \begin{bmatrix} 0 & \epsilon \end{bmatrix}^T \tag{26f}$$

B. On the accuracy of Taylor expansion for expressing delays

When using Taylor expansion to express time delay, it is in general not guaranteed that the remainder of (15); $R(t,\tau,N)$ is small [8]. In addition, higher order terms may not exist for the original delayed system. In fact, several sources warn against the usage of Taylor approximations to express time delays; see for example [9]. However for certain systems, when the delays are sufficiently small compared to the characteristic periods, the approximation may be useful. In addition, the expressed terms here are meant to provide insight into the effect of the delays, rather than expressing exact values. If a rational function approximations of time delays are needed for analysis, the Pade approximation [10], should be considered instead.

The delays investigated in this paper are generally small. Yet in order to assess how good the linear approximations are, a step displacement of 0.5m for M_1, on the system of (25) is now compared to the corresponding simulations performed in Simulink, using delay blocks and hold elements. In both tests the parameters indicated in Table I and II are used. The results are seen in Figure 7, and shows that the approximations are quite good for the given time delays.

C. Lessons from Approximation

Looking at the linear model of (25), we can now recognize that delayed linear stiffness forces lead to the introduction of linear damping forces, while delayed linear damping forces lead to the introduction of added mass terms in the system

Table I: Delays, ZOH's, and motor dynamics

Parameter	τ_1	τ_2	τ_3	τ_4	T_{d1}	T_{d2}	T_{d3}	T_{d4}	$h(s)$
Value	4ms	8ms	12ms	10ms	1.2ms	4ms	12ms	0ms	1

Table II: Simulation Parameters

Parameter	M_1	M_2	C_1	C_2	C_3	K_1	K_2	K_3	k_{tot}	ω_1	ω_2	ϵ
Value	1	1.2	0.05	0.1	0.05	8	6	12	40	0	0	0

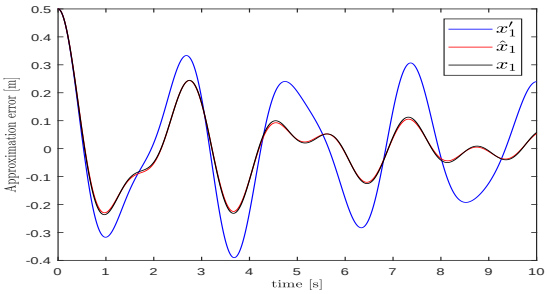

(a) Position of M_1

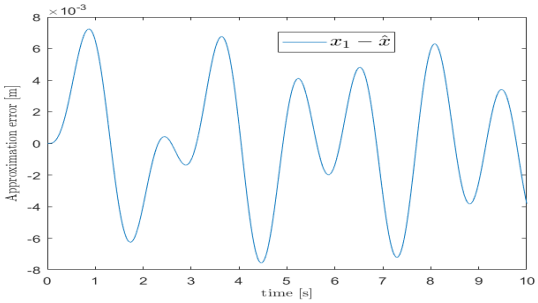

(b) Linear Approximation Error

Figure 7: Simulations using the values of Table I and II, where x_1 and $\hat{x}_1$ is the simulated and linearly approximated position of the mass. x_1' is the simulated position of the mass in an ideal system, where all time delays and ZOH of Table I of are set to zero.

equation. In fact, cross terms appear in the mass matrix, that previously were diagonal.

The dampening effect on the system, induced by the position cancellation term will typically be quite large, as the actuator stiffness is quite large. With the given values of Table I and II we have for $\boldsymbol{C}(1,1)$ of (26), that the damping term caused by the actuator stiffness is $K_{tot}(\tau_1'+\tau_4)=0.66\frac{Ns}{m}$, while the damping term from force reference feedforward is $-k_2(\tau_2'+\tau_3+\tau_4)=-0.22\frac{Ns}{m}$. The force reference feedforward term and the position cancellation terms thus have an opposite effect, where one extract energy and the other introduce energy. It is worth to realize that the damping coefficient $K_{tot}(\tau_1'+\tau_4)$ is independent on the system parameters. Thus the effect of the actuator delay will be somewhat less significant in real-time hybrid model testing, which typically has a larger mass relative to the movements of the structures than the case studied in this paper. A natural strategy to compensate for the effect of time delay is to include the linear error terms in the controller, thus canceling out the effect. This strategy would correspond to a linear prediction of the position and force estimates. Prediction is in fact commonly used for real-time hybrid applications. A much-used prediction scheme is to use polynomial based forward predictions schemes, see for example [7]. Prediction typically significantly reduce the effect of time delays, yet as it is difficult to estimate the delays accurately, it is difficult to fully eliminate their effect.

With the linear approximation, we can now also estimate what power the error we introduce to the system corresponds to:

$$\Delta\dot{E}_{err} \approx [\boldsymbol{M}_\tau \ddot{\boldsymbol{x}}]^T \dot{\boldsymbol{x}} + [\boldsymbol{C}_\tau \dot{\boldsymbol{x}}]^T \dot{\boldsymbol{x}} + \epsilon \dot{x}_1 \tag{27}$$

where $\boldsymbol{M}_\tau$ and $\boldsymbol{C}_\tau$ are the delay dependent part of the matrices of (26)

V. Full System Analysis

In this section, we will do more in-depth simulations, where the delays and ZOH are estimated through transport delay blocks and hold elements and simulated in Simulink.

A. Energy Considerations

Figure 8 investigates what effect the hybrid system has on the energy of the system, for the same step-test as performed in Figure 7. The figure separates between the energy contributions from the four different terms; ΔF_{num}, $(F_c - F_{ff})$,F_{fx} and the physical damping.

As may be expected, it is clear that the position cancellation term will drain energy from the system, while the contributions from the force reference feedforward and numerical substructure introduce energy to the system. With the given parameters, as indicated before, we have that the position cancellation term is the most dominant term when it comes to damping energy from the system.

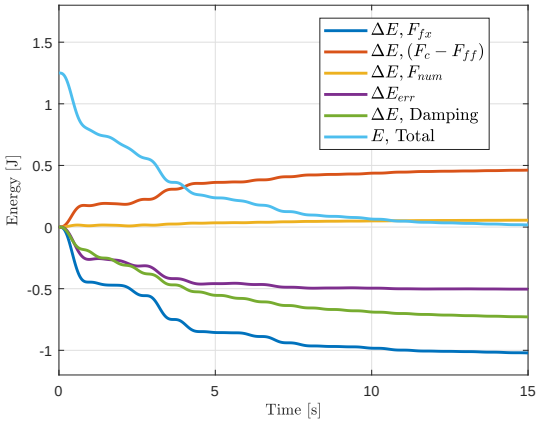

Figure 8: Energy of the system for a step test using the simulation parameters of Table II, and I. ΔE represents the cumulative energy introduced or extracted from the corresponding term, ΔE_{err} is the sum of energy introduced or extracted by the hybrid system, and E-Total is the total energy (kinetic + potential) of the system.

B. Trajectories and energy with different time delays

The effect of different time delays will now be studied, performing simulations where the parameters of Table I are multiplied by a scalar factor. The resulting position of M_1 can be seen in Figure 9a, while the total energy left in the system is plotted in Figure 9b. Not surprisingly there is a clear correlation between the level of time delays and the accuracy of the hybrid system. In this case the energy extractive-terms seem to dominate the introduced energy-terms.

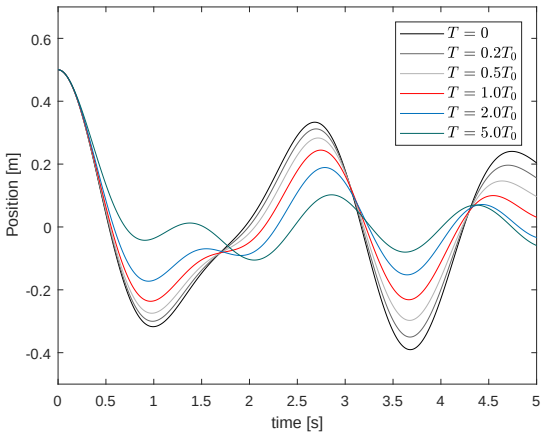

(a) Position of M_1

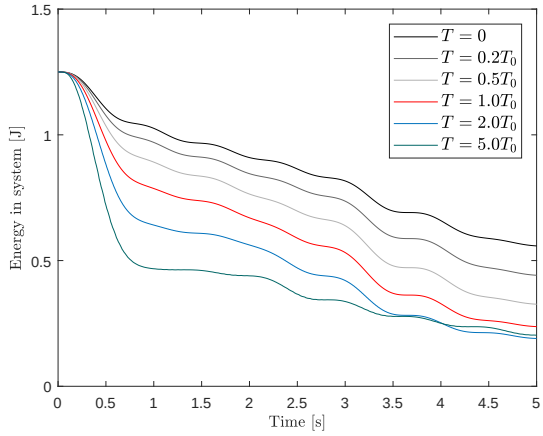

(b) Energy in System

Figure 9: Effect of time delays for a step-test of 0.5m on position of M_1. T_0 represents the time variables as given in Table I, while T is a scaled version of the same parameters. $T = 0$ correspond to the ideal system.

C. Effect of one millisecond position cancellation delay

In this test, the physical damping, time delays and ZOH elements are all set to zero. The effect of 1 ms delay on the position cancellation term (τ_1) is subsequently investigated through simulations of a step test with M_1 initialized at 0.5 m, as seen in Figure 10. The test is performed for two values of the actuator stiffness, $K_{tot} = 40\frac{N}{m}$ and of $K_{tot} = 140\frac{N}{m}$ respectively. $K_{tot} = 140\frac{M}{m}$ is the estimated stiffness of the actuator used in hybrid testing in [2, Sec 13.3.2]. As can be seen in the figure, the damping effect is considerable, even with only 1ms delay.

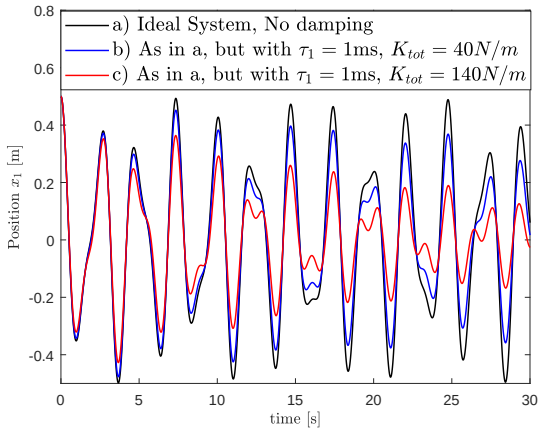

Figure 10: Step test with no damping terms, Mass and stiffnesses are given in Table II.

D. Excited System

We will now consider the case where the system is excited by external forces. The system equations of (8) are first expressed through the Laplace transform as follows:

$$\frac{\boldsymbol{x}}{\boldsymbol{F}}(s) = \frac{1}{(\boldsymbol{M}(s)s^2 + \boldsymbol{C}(s)s + \boldsymbol{K}(s))} \tag{28}$$

where

$$\boldsymbol{M} = \begin{bmatrix} M_1 & 0 \\ 0 & M_2 \end{bmatrix} \tag{29a}$$

$$\boldsymbol{C} = \begin{bmatrix} c_1 + c_2 h(s) e^{-\tau_{234} s} & -c_2 h(s) e^{-\tau_{34} s} \\ -c_2 e^{-(\tau_2 s)} & c_2 + c_3 \end{bmatrix} \tag{29b}$$

$$\boldsymbol{K} = \begin{bmatrix} k_1 + k_{tot}(1 - h(s) e^{-\tau_{14} s}) + k_2 h(s) e^{-(\tau_{234} s)} & -k_2 h(s) e^{-(\tau_{34} s)} \\ -k_2 e^{-(\tau_2 s)} & k_2 + k_3 \end{bmatrix} \tag{29c}$$

$$\boldsymbol{F} = \begin{bmatrix} \omega_1 \\ \omega_2 \end{bmatrix} \tag{29d}$$

$$\tag{29e}$$

and

$$\tau_{234} = \tau_2 + \tau_3 + \tau_4 \tag{30a}$$

$$\tau_{14} = \tau_1 + \tau_4 \tag{30b}$$

$$\tau_{34} = \tau_3 + \tau_4 \tag{30c}$$

Here, $e^{-\tau s}$ is the Laplace transform of a delay τ. Note that for simplicity the ZOH-elements have not been included in this analysis.

Using the values for $\boldsymbol{M}, \boldsymbol{C}$, and $\boldsymbol{K}$ given by Table II, and the time delays given in Table I, a Bode plot matrix is now generated between the system input $\begin{bmatrix} \omega_1 & \omega_2 \end{bmatrix}^T$ and system outputs $\begin{bmatrix} x_1 & x_2 \end{bmatrix}^T$. The Bode plot matrix is given in Figure 13.

In order to verify the results of the bode-plot, and to get an idea of how the system acts in the transient part, two

Table III: Frequency response, as read by the Bode plot, at sample points

	$f_1 = 1$rad/s	$f_1 = 2.4$ rad/s
Amplitude Ideal System	0.146	0.96
Amplitude Hybrid System	0.145	0.54

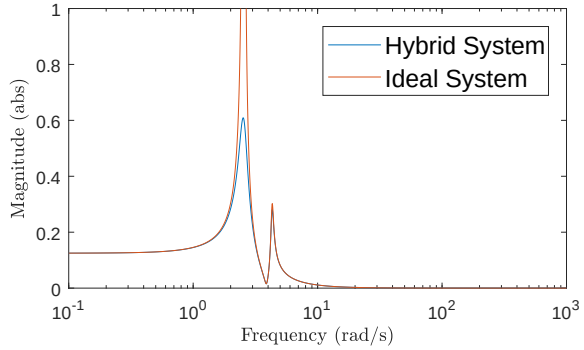

Figure 11: Bode plot from ω_1 to x_1 (Magnitude scale: abs)

simulations is performed, both initialized at equilibrium, with the external force ω_1 being a harmonic force of amplitude one and frequencies of $1\frac{\text{rad}}{\text{s}}$ and $2.4\frac{\text{rad}}{\text{s}}$ respectively. Note that the frequency of $2.4\frac{\text{rad}}{\text{s}}$ is near the resonance frequency, while $1\frac{\text{rad}}{\text{s}}$ is not near resonance frequencies.

The steady state response that we would expect from simulations using these harmonic excitations forces (according to the Bode plot) is given in Table III. The simulated responses are given by Figure 12. Comparing Figure 11 and Table III, we can see that, as expected, the steady-state response correspond well between the Bode plot and the two simulations.

As can be seen, both in the Bode plots and simulations, the delayed system yields quite accurate steady state response in frequencies outside the natural frequencies of the system. At the natural frequencies, however, the induced damping will play a significant role in reducing the achieved amplitudes.

VI. Conclusions

As the paper shows, even small delays may cause a significant effect on the performance of the hybrid test setup. This is especially true for the test case studied in this paper, which due to its relatively small dimensions (in terms of mass and stiffnesses relative to movements) is heavily affected by the position cancellation term, which induces a damping.

As a result of the time delays, the test case is shown to behave quite poorly at replicating decay tests, where the system is initialized at given position, whilst when subjected to harmonic excitation forces, we achieve better replication as long as the forces are outside the natural frequency of the system.

If possible, delays and sampling periods should be kept small in order to reduce their effect on the system. As they are difficult to eliminate, it is advised to do some form of forward prediction to reduce their effect.

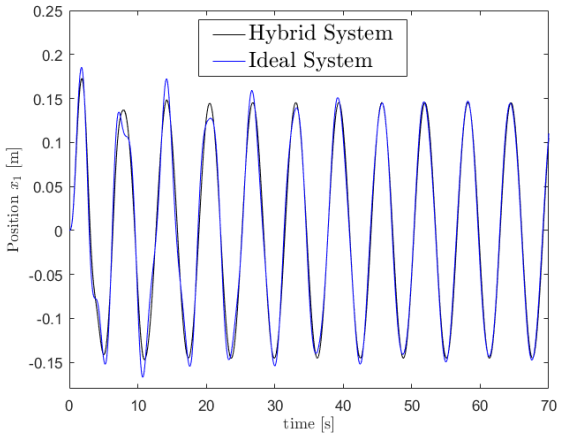

(a) $\omega_1 = sin(1t)$

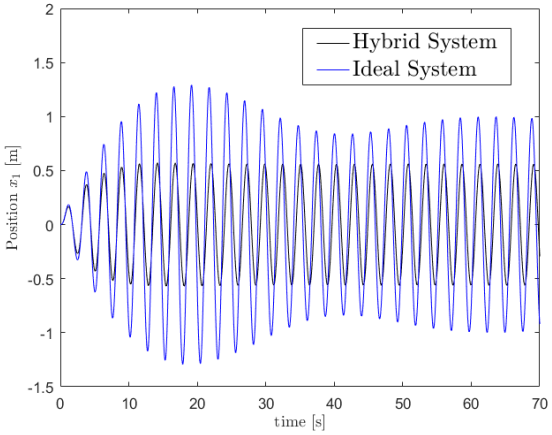

(b) $\omega_1 = sin(2.4t)$

Figure 12: Harmonic excitations forces applied to the system. Ideal system versus hybrid system.

VII. Further studies

The simple experimental setup of Figure 3, with interchangeable spring and mass elements connected to the actuator, has been developed, complete with sensors, real-time computers and data data acquisition systems. Future research is planned at a later stage, based on experimental testing using this setup.

VIII. Acknowledgment

The presented work was support of the HYBRID KPN project supported by the Maritime Activities and Offshore Operations Program (MAROFF) of the Research Council of Norway (grant No. 254845/O80). The work was also supported by the Centre of Excellence AMOS, project no. 223254

References

[1] S. A. Vilsen, T. Sauder, and A. J. Sørensen, "Real-time hybrid model testing of moored floating structures using nonlinear finite element simulations," in *Dynamics of Coupled Structures, Volume 4*. Springer, 2017, pp. 79–92.

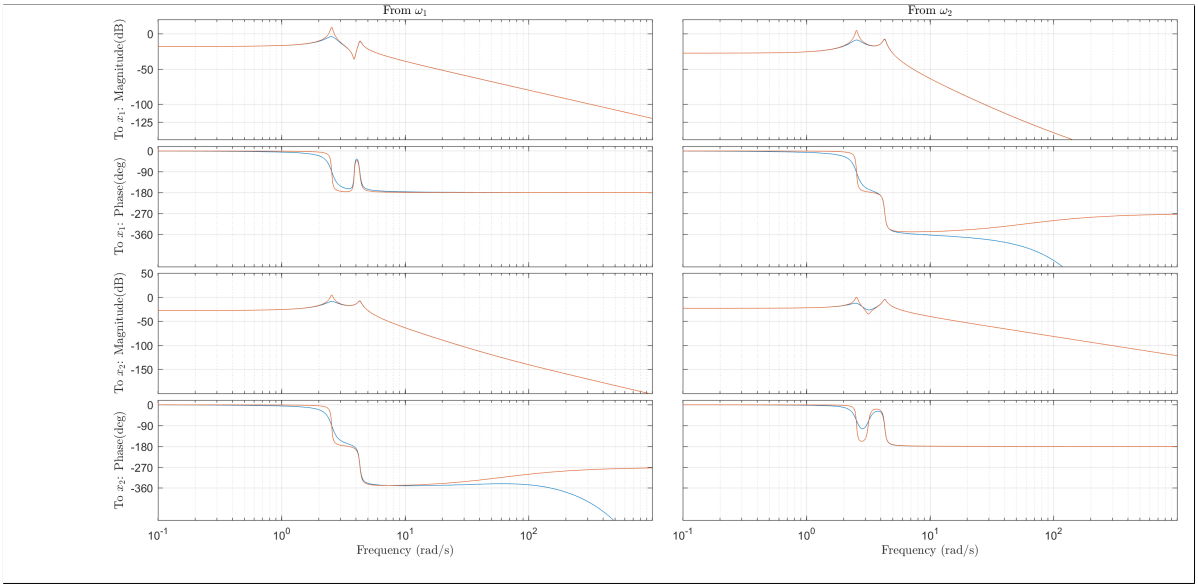

Figure 13: Bode plot from $[\omega_1, \omega_2]^T$ to $[x_1, x_2]$ (Magnitude scale: dB)

[2] V. Chabaud, "Real-time hybrid model testing of floating wind turbines," Ph.D. dissertation, Norwegian University of Science and Technology., 2016.

[3] C. T. Stansberg, H. Ormberg, and O. Oritsland, "Challenges in deep water experiments: hybrid approach," *Journal of Offshore Mechanics and Arctic Engineering*, vol. 124, no. 2, pp. 90–96, 2002.

[4] T. Sauder, A. Sørensen, and K. Larsen, "Real-time hybrid model testing of a top tensioned riser: A numerical case study on interface time-delays and truncation ratio," in *Proceedings of the 36th International Conference on Ocean, Offshore and Arctic Engineering Trondheim, Norway (OMAE2017)*, 2017.

[5] T. Sauder, V. Chabaud, M. Thys, E. Bachynski, and L. O. Sæther, "Real-time hybrid model testing of a braceless semi-submersible wind turbine: Part I. the hybrid approach," in *Proceedings of the 35th International Conference on Ocean, Offshore and Arctic Engineering*, 2016.

[6] O. Egeland and J. T. Gravdahl, *Modeling and simulation for automatic control*. Marine Cybernetics Trondheim, Norway, 2002, vol. 76.

[7] M. Wallace, D. Wagg, and S. Neild, "An adaptive polynomial based forward prediction algorithm for multi-actuator real-time dynamic sub-structuring," in *Proceedings of the Royal Society of London A: Mathematical, Physical and Engineering Sciences*, vol. 461, no. 2064. The Royal Society, 2005, pp. 3807–3826.

[8] T. Insperger, "On the approximation of delayed systems by taylor series expansion," *Journal of Computational and Nonlinear Dynamics*, vol. 10, no. 2, p. 024503, 2015.

[9] A. Mazanov and K. P. Tognetti, "Taylor series expansion of delay differential equationsa warning," *Journal of theoretical biology*, vol. 46, no. 1, pp. 271–282, 1974.

[10] A. George Jr *et al.*, *Essentials of Padé approximants*. Elsevier, 1975.